Eur. Phys. J. D **31**, 205–211 (2004)
DOI: 10.1140/epjd/e2004-00156-5

THE EUROPEAN PHYSICAL JOURNAL D

Spectroscopic studies of NaCs for the ground state asymptote of Na + Cs pairs*

O. Docenko[1], M. Tamanis[1], R. Ferber[1], A. Pashov[2], H. Knöckel[3], and E. Tiemann[3,a]

[1] Department of Physics and Institute of Atomic Physics and Spectroscopy, University of Latvia, Rainis Boulevard 19, LV 1586 Riga, Latvia
[2] Institute for Scientific Research in Telecommunications, ul. Hajdushka poliana 8, 1612 Sofia, Bulgaria
[3] Institut für Quantenoptik, Universität Hannover, Welfengarten 1, 30167 Hannover, Germany

Received 29 June 2004 / Received in final form 10 September 2004
Published online 23 November 2004 –

Abstract. The ground state $X^1\Sigma^+$ of NaCs was studied by laser induced fluorescence Fourier-transform spectroscopy. An accurate potential energy curve was derived from more than 5000 transitions. This potential reproduces the experimental observations within their uncertainties of ± 0.003 cm^{-1} and covers about 99.97% of the potential well depth. Few vibrational levels of the shallow state $a^3\Sigma^+$ below the atomic ground state asymptote were observed. The identification is mainly done by the observed and quantitatively interpreted molecular hyperfine structure applying atomic parameters of the ground states of Na and Cs. An estimated potential curve for $a^3\Sigma^+$ is reported which can be used together with that of $X^1\Sigma^+$ for coupled channel calculations of cold collisions between Na and Cs. An example is given.

PACS. 31.50.Bc Potential energy surfaces for ground electronic states – 33.20.Kf Visible spectra – 33.20.Vq Vibration-rotation analysis – 33.50.Dq Fluorescence and phosphorescence spectra

1 Introduction

The heteronuclear alkali dimers attract interest of both experimental and theoretical researchers involved in collision dynamics at threshold, photoassociative spectroscopy, laser cooling and trapping of alkali atoms [1–4]. Special interest is put on the study of the ground states and especially near the atomic asymptote, since the precise knowledge of the long-range interactions between two different types of alkali atoms is necessary for understanding and realization of cold collision processes like sympathetic cooling, formation of two species BEC (TBEC) and ultracold heteronuclear molecules. Polar species are presently discussed in relation to ultracold molecular ensembles determined by the anisotropic dipole-dipole interaction, and new possibilities of highly correlated many-body quantum systems are expected, e.g. BCS-like superfluids [5] or supersolids and checkerboard states [6]. Hence, there is an acute need for detailed knowledge of the heteronuclear alkalis and the determination of precise potentials in a wide range of internuclear distances close to the atomic asymptote. Recent success in the photoassociation of hetero alkalis, like RbCs [7], demand for detailed electronic spectroscopic studies to get better predictions for further experiments.

An extensive theoretical study of the electronic structure of NaCs has been performed [8]. Potential energy curves (PEC) for 32 electronic states were calculated far out to the atomic asymptotes. Selected low electronic states from reference [8] are shown in Figure 1 for better understanding of electronic assignment of transitions involved in the present experiment. Because we are interested in $X^1\Sigma^+$ and $a^3\Sigma^+$ states the figure contains only states with symmetries $^1\Sigma^+$, $^3\Sigma^+$, $^1\Pi$ and $^3\Pi$ the excitation of which will lead to decay to the ground state manifold.

Accurate experimental spectroscopic information on NaCs is still limited, including that for the ground state. A combination of polarization spectroscopy and optical double-resonance methods in reference [9] has provided precise data for the lowest part of the ground state limited to vibrational quantum numbers $v'' \leq 21$, and measurement of laser-induced fluorescence by means of a grating spectrograph yielding data for higher levels up to $v'' = 64$. Combined analysis of these data gave Dunham coefficients, RKR potential and an estimate of the dissociation energy $D_e = 4950 \pm 100$ cm^{-1} of the ground state $X^1\Sigma^+$. Kopystynska et al. [10] studied the laser induced fluorescence spectroscopy in a cell with different mixtures of alkalis. Exciting with Ar^+ laser at 514.5 nm

* Supplementary tables (Tabs. I–III) are only available in electronic form at `http://www.eurphysj.org`

[a] e-mail: `tiemann@iqo.uni-hannover.de`

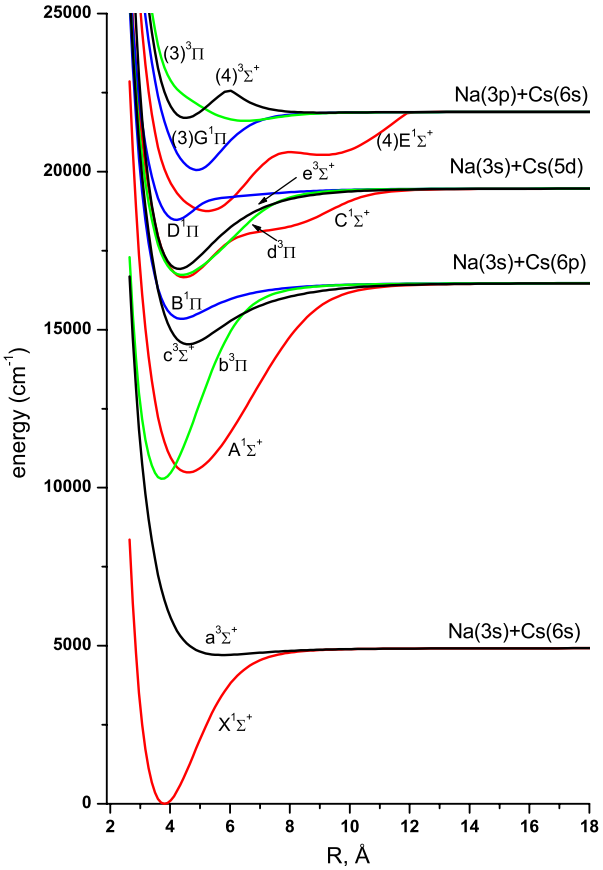

Fig. 1. Low singlet and triplet electronic states in NaCs according to reference [8].

they found several progressions one of which in the red (around 660 nm) they identified as progression of NaCs to $a^3\Sigma^+$. Because of fairly low resolution they used several indirect arguments for this identification.

The goal of the present investigation is to study the ground $X^1\Sigma^+$ electronic state of NaCs in a wide range of internuclear distances with the help of the Fourier-transform spectroscopy which has proven itself as a very powerful tool for accurate studies of the ground states of Ca_2 and NaRb [11,12], reaching the long range region of the potential. The second goal is to search for spectral structures of the triplet state correlating to the atomic ground state asymptote Na($3s$) + Cs($6s$) which one needs for the full description of ultracold collisions between Na and Cs with their resonance structure, which might reveal new ways for producing ultracold polar molecules and ensembles of them, opening ways of highly correlated systems [5,6] by interacting electric or magnetic dipole moments.

2 Experiment

In order to ensure safe operation with Cs a metal cell was designed. The 300 mm long cell has approximately 30 mm in diameter and CF flanges are welded at both ends for mounting sapphire windows (Varian Vacuum Technologies). A metal container is appended at the side of the cell for two ampullas with 1 g Na and 1g Cs and closed by a CF flange. The end of the Na ampulla was cut just before the loading. The cell is connected to the vacuum apparatus via a metal bellows-all-welded valve from Swagelock welded to the cell. In this configuration the whole cell (including the windows, container and the metal valve) can be heated up to 700 K. After the cell was pumped for several days at temperatures up to 400 K, low enough for not losing the Na, the Cs ampulla was broken by shaking the cell. The advantages of using the metal cell compared to the traditional heat-pipe ovens are the safe procedures for loading, the possibility for operation with small amounts of metals, and also without presence of buffer gas. At the same time the metal cell has some advantages over the glass cells since all connections are realized with CF flanges. Usually the cell was heated to 550–600 K and operated without buffer gas.

Unfortunately, after about 20 hours of operation a leak in the sapphire windows of the cell was found. It should be investigated whether it happened due to bad quality of the welding between the sapphire and the metal of CF flange or due to general non resistance of this welding to alkali metal vapors.

For longer experimental studies a heat-pipe oven was designed similar to that described in reference [11] which was provided with a short metal container welded to the central part of the pipe. A 5 g glass ampulla of Cs from Alfa Aesar was loaded in the container and closed with a CF flange. About 10 g of Na were loaded in the heat-pipe in a usual way. After several days of conditioning, the Cs ampulla was broken by shaking the heat-pipe oven. Since the container was mounted close to the pipe and heated simultaneously with it up to the same temperature, the heat-pipe was operated in a simple single section heat-pipe regime, rather than as an injection heat-pipe (see e.g. Ref. [13]). The oven was operated at temperatures between 560 K and 600 K and typically with 3 mbar of Ar as a buffer gas. The oven was in operation for about 50 hours without refilling and at the end of the experiment it was still in good working condition.

Strong laser induced fluorescence (LIF) was observed when the sample was illuminated with Ar^+ laser operated at lines: 514.5, 496.5, 488.0, 476.5 nm (single mode, typical power 100÷500 mW) and by a single-mode dye laser (Coherent 699-21) with Rhodamine 6G dye (typical power at the sample 150 mW). This allowed us to observe the $G^1\Pi$–$X^1\Sigma^+$, $D^1\Pi$–$X^1\Sigma^+$ and $E^1\Sigma^+$–$X^1\Sigma^+$ band systems in NaCs along with Na_2 progressions. As the working temperatures were relatively low, the Na_2 signals were weak and did not disturb the measurement and the identification of the NaCs bands. Pure Cs_2 bands were not observed during these experiments. The frequency of the Rhodamine 6G laser was varied between 17527 cm^{-1} and 17768 cm^{-1} which allowed us to record and assign about 40 D–X and 10 E–X progressions.

The assignment $G^1\Pi$ and $D^1\Pi$ as origins for the progressions becomes clear by the appearances of Q

progressions ($\Delta J = 0$). Due to a considerable extension of the $E^1\Sigma^+$ potential in internuclear separation, see Figure 1, it was possible to observe transitions to high vibrational levels of the ground state (up to $v'' = 83$) close to the dissociation limit.

Additionally, we observed a LIF progression at excitation frequency 15538.4 cm^{-1} (DCM dye). According to the potential scheme in Figure 1 this progression could be assigned as $B^1\Pi$–$X^1\Sigma^+$ transitions.

The fluorescence from the oven was collected in the direction opposite to the propagation of the laser beam and then imaged to the input aperture of Bruker IFS 120 HR Fourier spectrometer. The signal was detected with a Hamamatsu R928 photomultiplier tube or a silicon diode depending on the desired wavelength. The scanning path of the interferometer was set to reach typical resolutions of 0.015–0.03 cm^{-1} and the number of scans for averaging varied between 5 and 10. In order to avoid the illumination of the detector by the He–Ne laser, used in the spectrometer for calibration and stepping control, we set a Notch filter with FWHM 8 nm in the optical path. For better signal-to-noise ratio some spectra were recorded by limiting the desired spectral window with color glass or interference filters. Some progressions were recorded several times to check the internal consistency; in these cases progressions show sometimes a systematic shift of up to 0.02 cm^{-1} against each other which simply relates to the Doppler shift resulting from the selected excitation wavelength for the individual progression. Nevertheless the relative positions of the strong spectral lines within a progression were estimated to be accurate to at least ± 0.003 cm^{-1}.

All transitions excited in NaCs by the Ar^+ and dye laser are listed in Table I of the supplementary *Online material*, including the assignment of the present analysis. Table II of the supplementary *Online material* contains the observed fluorescence progressions.

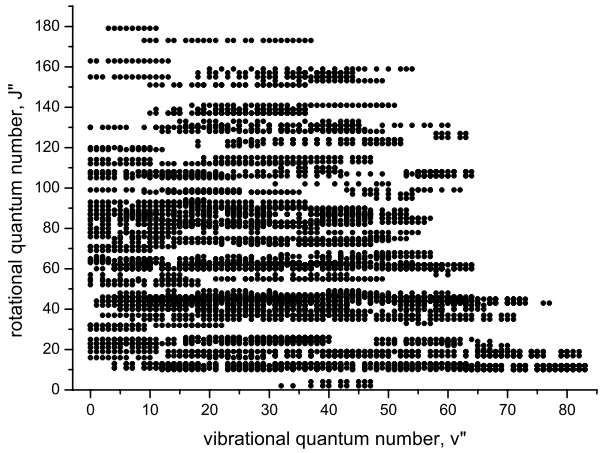

Fig. 2. The range of vibrational and rotational quantum numbers of the observed ground state energy levels in NaCs.

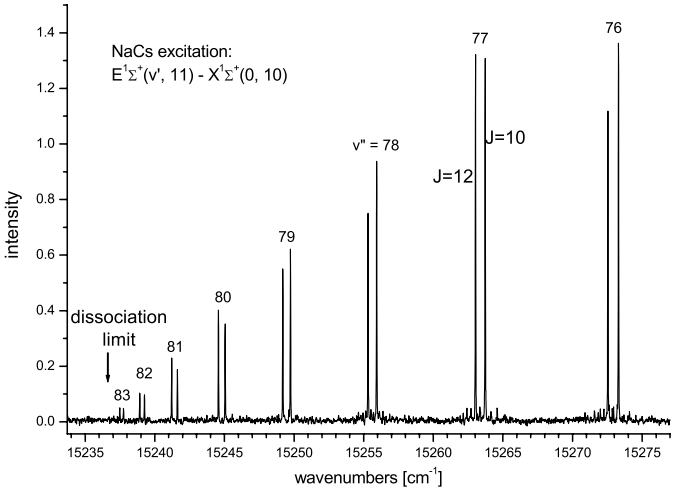

Fig. 3. The vibrational progression up to $v'' = 83$ in NaCs excited by a single mode Ar^+ laser line 496.5 nm.

3 Analysis of the ground state

The assignment of the recorded spectra was simplified by the published potential energy curve in reference [9]. After we identified the strongest progressions, a new potential was fitted. This preliminary potential was further improved adding more newly collected experimental data in the fit; this sequential procedure allows continuous checking of the assignment, especially for high J'' and in cases of gaps in v''. The total data set (Fig. 2) consists of more than 5000 transitions corresponding to 2892 different ground state levels in NaCs.

Figure 3 gives a short section of the many recordings to show the quality of data and also the reliability of the extrapolation to the atomic ground state asymptote; the last observed level is $v'' = 83$. This progression is specifically selected for this figure as an example with low $J'' = 0, 12$ to reduce the influence of the centrifugal potentials in the energy scale very much getting a fairly good extrapolation to the dissociation limit as indicated in the figure. The calculation with the potential derived below predicts that $v'' = 84$ would be the last bound vibrational level for these J'' values.

For the construction of the PEC for the ground state, we set-up an analytic potential with which we solve numerically the radial Schrödinger equation. The potential is represented as a truncated expansion over analytic functions [14]:

$$U(R) = \sum_{i=0}^{n} a_i \left(\frac{R - R_m}{R + bR_m} \right)^i \quad (1)$$

where a_i, b and R_m are parameters (R_m is close to the equilibrium distance). This analytic form is used in the interval $R_i < R < R_o$. For the long range region $R \geq R_o$ the expression is applied:

$$U_{\mathrm{LR}}(R) = D_{\mathrm{e}} - C_6/R^6 - C_8/R^8 - C_{10}/R^{10} - \ldots \quad (2)$$

D_{e} is adjusted to continuously connect the analytic branch to the long range branch. Note that this formula will be extended as given in equation (4) for describing the long range behavior of the singlet and triplet state properly.

For short internuclear distances $R \leq R_i$ the potential is smoothly extended with the ansatz:

$$U_{\mathrm{SR}}(R) = A \exp(-B(R - R_i)). \quad (3)$$

Our method determines the potential curves directly from the experimental observations and the accuracy of a derived PEC is evaluated by comparing the differences between calculated energy levels with the experimental differences in the progression (see Refs. [11,12]). The uncertainty of the experimental differences is estimated from the instrumental resolution and the signal-to-noise ratio of the involved spectral lines. The potential parameters are determined by well-known non-linear least squared methods (for details see [14]).

Initially, it was decided that only a_i for equation (1) had to be determined during the fitting procedure. C_6, C_8 and C_{10} were fixed to their most recent theoretical values from references [15,16], while A, B and D_{e} were adjusted by the program in order to ensure proper connection between the extensions and the analytic form. R_m, b and the connecting points R_i and R_o were kept fixed to values, which allow fast convergence of the fitting routine.

For the fit 29 potential coefficients according to equation (1) were used which allowed to fit almost all observations within experimental accuracy, only levels with turning point around 12 Å or larger show systematic deviations. Thus it was checked which is the most appropriate long range parameter for taking this deviation into account. Including only C_6 gives the most significant improvement and also decreases its value compared to the theoretical prediction of reference [16] by less than 1%. But we will not claim that we derived from our data set a more reliable C_6 coefficient. The correlation to the higher order dispersion parameters is large and thus the different terms are not really distinguishable. Table 1 gives the derived parameters for the full potential for the fit with normalized standard deviation $\sigma = 0.88$. Error limits for the individual potential parameters are not estimated, because they do not have any individual physical meaning. Using the potential, eigenvalues from the radial Schrödinger equation can be derived in the quantum number limits according to the overview in Figure 2 with an averaged accuracy of better than 0.003 cm^{-1}.

In Table III of the supplementary *Online material* we provide also the result of a potential fit using a pointwise potential representation with natural cubic spline interpolation. The fit quality is similar but 50 parameters were included in that fit. This table might help different research groups who have a working numerical code for energy level calculation which can directly read in this potential representation.

Our previous experience showed that for molecules with reduced masses similar to that of NaCs [11,12] the Born-Oppenheimer breakdown corrections in the ground state may be neglected at the considered level of accuracy even for data sets including several isotopic species and relatively high J quantum numbers. These corrections are however certainly of importance for highly accurate data [17] or light molecules [18].

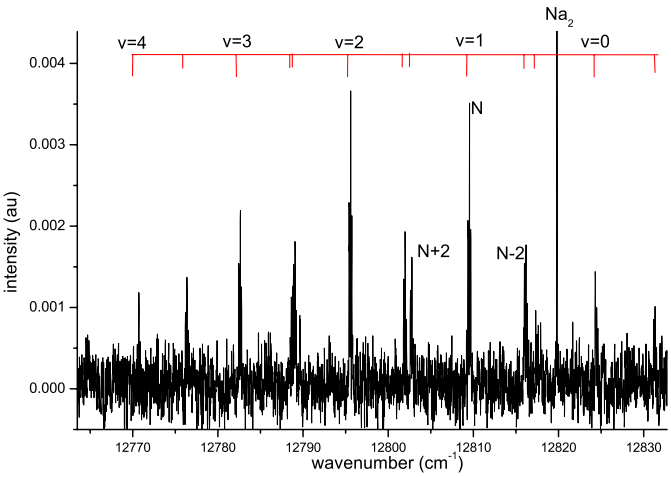

Fig. 4. A vibrational progression of $a^3\Sigma^+$ in NaCs excited by the dye laser at 17344 cm^{-1}, $N = 73$ is the rotational quantum number in Hund's case (b).

In the traditional way we performed fits of the observed energy levels by the Dunham power expansion with the coefficients Y_{ik} where i and k are the powers of $(v+1/2)$ and $J(J+1)$, respectively. The fit gives a normalized standard deviation of $\sigma = 0.73$, comparable to the result of the potential fit. This representation of all energy levels by 56 parameters Y_{ik} is contained in Table III of the supplementary *Online material* and will give more reliable calculations of energy levels compared to those Y_{ik} reported in reference [9] because of their limited data set.

4 Search for the triplet state

Figure 1 shows that there could be coupling between $C^1\Sigma^+$ and a triplet state. Thus exciting an appropriate level a decay to the triplet ground state $a^3\Sigma^+$ with its very shallow potential could become observable. We were successfully searching for such possibility and Figure 4 shows a short progression, when exciting at 17344 cm^{-1}. The identification was first done by an energy location of this progression which comes close to the energy of the atomic ground asymptote $3s + 6s$ and second, the small vibrational spacing of about 15 cm^{-1} being close to the expected value from level calculations with the electronic potential of $a^3\Sigma^+$ taken from reference [8].

A zoom of any single transition in Figure 4 shows hyperfine structure which one can simulate with a coupled channel calculation (see e.g. Ref. [14]), plugging in the ground state potential $X^1\Sigma^+$ as given in Table 1, the ab initio potential of $a^3\Sigma^+$ [8], shifted to the same asymptotic energy as of $X^1\Sigma^+$ and using the atomic hyperfine splittings of Na and Cs compiled in [19]. Figure 5 shows the observed spectrum and the calculated hyperfine structure as a bar pattern with fixed length, because simulating relative intensities is not yet possible in the absence of assignments for the excited coupling states. However the energy splitting is convincingly reproduced, leaving no doubt that this progression ends at the desired state $a^3\Sigma^+$.

Table 1. Parameters of the analytic representation of the potential energy curve of the $X^1\Sigma^+$ state in NaCs.

for $R \leq 2.80$ Å	
R_i	2.80 Å
A	5509.4338 cm^{-1}
B	1.5020227100 $Å^{-1}$
for 2.80 Å $< R <$ 12.70 Å	
b	–0.4000
R_m	3.85062906 Å
a_0	0.0 cm^{-1}
a_1	1.29677346150536610 cm^{-1}
a_2	$1.51728492476490264 \times 10^4$ cm^{-1}
a_3	$1.09095191433899363 \times 10^4$ cm^{-1}
a_4	$-2.45806495177720808 \times 10^3$ cm^{-1}
a_5	$-1.60799862149231794 \times 10^4$ cm^{-1}
a_6	$-8.70962559205579782 \times 10^3$ cm^{-1}
a_7	$2.18747535596727575 \times 10^4$ cm^{-1}
a_8	$-3.00243720449833432 \times 10^5$ cm^{-1}
a_9	$-7.86930451496603433 \times 10^5$ cm^{-1}
a_{10}	$3.39616970842697797 \times 10^6$ cm^{-1}
a_{11}	$7.35841534829050489 \times 10^6$ cm^{-1}
a_{12}	$-2.63747919952689409 \times 10^7$ cm^{-1}
a_{13}	$-4.45851005134318396 \times 10^7$ cm^{-1}
a_{14}	$1.35133654058888495 \times 10^8$ cm^{-1}
a_{15}	$1.76262769398831815 \times 10^8$ cm^{-1}
a_{16}	$-4.75687836575036168 \times 10^8$ cm^{-1}
a_{17}	$-4.47488337869063497 \times 10^8$ cm^{-1}
a_{18}	$1.21600041878172946 \times 10^9$ cm^{-1}
a_{19}	$7.46075675097115278 \times 10^8$ cm^{-1}
a_{20}	$-2.29173360205131388 \times 10^9$ cm^{-1}
a_{21}	$-8.70893719909687042 \times 10^8$ cm^{-1}
a_{22}	$3.09544150282176447 \times 10^9$ cm^{-1}
a_{23}	$8.19954467973030806 \times 10^8$ cm^{-1}
a_{24}	$-2.80675453436517239 \times 10^9$ cm^{-1}
a_{25}	$-6.96373081872487426 \times 10^8$ cm^{-1}
a_{26}	$1.51653594722299957 \times 10^9$ cm^{-1}
a_{27}	$4.44558531531333089 \times 10^8$ cm^{-1}
a_{28}	$-3.66990684866598368 \times 10^8$ cm^{-1}
a_{29}	$-1.35242647548431933 \times 10^8$ cm^{-1}
for $R \geq 12.70$ Å	
R_o	12.700 Å
D_e atomic asymptote	4954.1847 cm^{-1}
C_6	1.550513×10^7 $cm^{-1}Å^6$
C_8	4.88540×10^8 $cm^{-1}Å^8$
C_{10}	1.7170×10^{10} $cm^{-1}Å^{10}$
A_{ex}	2.834990×10^4 $cm^{-1}Å^{-\gamma}$
γ	5.12271
β	2.17237 $Å^{-1}$

The next step should be to assign the quantum numbers of this progression. For this purpose we searched carefully to find a corresponding singlet progression to the X state from the excited state which should be a mixed singlet-triplet state. But within the achieved sensitivity we were unable to identify without doubt such series; only short singlet series were found which originate from accidentally overlapping excitations. Thus we used the ab initio potential, scaled to accommodate the observed

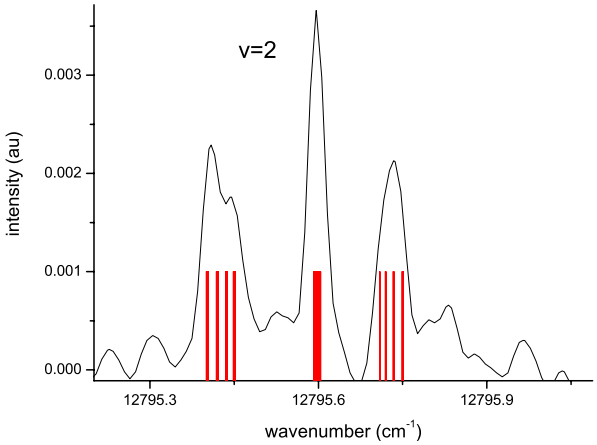

Fig. 5. Observed hyperfine structure in $a^3\Sigma^+$ of NaCs and coupled channel simulation using atomic hyperfine splittings of Na and Cs ground state.

short progression with the smallest changes compared to the theoretical one. This is possible with the vibrational quantum numbers given in Figure 4 and rotational quantum number $N = 73$, according to an assumed Hund's coupling case b for $a^3\Sigma^+$. For each vibrational level three rotational levels with N and $N \pm 2$ are observed which is compatible with a mixed $^3\Pi$ state, from the excitation energy probably $d^3\Pi$. But obviously no resonance coupling to the adjacent $C^1\Sigma^+$ is involved, which would give another rotational structure of the progression then observed.

An estimation of the exchange force term of the long range behavior was obtained by fitting the interval of 9.0 Å to 12.7 Å of the ground state $X^1\Sigma^+$ to the form:

$$U_{\rm LR}(R) = D_{\rm e} - C_6/R^6 - C_8/R^8 - C_{10}/R^{10} - A_{ex}R^{\gamma}\exp(-\beta R). \quad (4)$$

β and γ are estimated as discussed for heteronuclear species by [4] from the atomic ionization energies of Na and Cs. The values are shown in Table 1 because the exchange energy was incorporated also in the final fit of the ground state observations. Table 2 contains the scaled ab initio potential parameters of $a^3\Sigma^+$ which are consistent with the observed progression and which can be further used in coupled channel calculations for modeling cold collisions. Such model calculation will also be used for predicting search regions for the triplet spectroscopy to obtain sufficient data for deriving the potential of $a^3\Sigma^+$ with the same quality as for $X^1\Sigma^+$.

The construction of this potential, namely the connection to the common asymptote with the ground state $X^1\Sigma^+$, which fixes the levels of $X^1\Sigma^+$and $a^3\Sigma^+$on the absolute energy scale, can be checked by using the excitation of 17344.705 cm^{-1} for the observation of the progression in Figure 4 and identifying the ground state level from which this excitation originates. This calculation results to a term energy of this level 360.73 cm^{-1} with respect to the minimum of the potential curve of $X^1\Sigma^+$. This is only 0.96 cm^{-1} above $v'' = 0$ $J'' = 73$ of $X^1\Sigma^+$ and such

Table 2. Parameters of the estimated potential of the $a^3\Sigma^+$ state of NaCs.

for $R \leq 4.65$ Å	
R_i	4.65 Å
A	5037.8137 cm^{-1}
B	0.154308628 $Å^{-1}$
for 4.65 Å $< R <$ 9.10 Å	
b	0.0
R_m	5.75585938 Å
a_0	4738.4097 cm^{-1}
a_1	9.50863534122557574 cm^{-1}
a_2	$3.56716196426992701 \times 10^3$ cm^{-1}
a_3	$-7.27600667601568057 \times 10^3$ cm^{-1}
a_4	$2.76969524369466626 \times 10^3$ cm^{-1}
a_5	$2.25463633633282961 \times 10^3$ cm^{-1}
a_6	$-2.82403322359167178 \times 10^4$ cm^{-1}
a_7	$5.74785812916924697 \times 10^4$ cm^{-1}
a_8	$1.56272523166551022 \times 10^5$ cm^{-1}
a_9	$-3.64121347650245181 \times 10^5$ cm^{-1}
for $R \leq 9.10$ Å	
R_o	9.10 Å
D_e atomic asymptote	4954.1847 cm^{-1}
C_6	1.550513×10^7 $cm^{-1}Å^6$
C_8	4.88540×10^8 $cm^{-1}Å^8$
C_{10}	1.7170×10^{10} $cm^{-1}Å^{10}$
A_{ex}	-2.834990×10^4 $cm^{-1}Å^{-\gamma}$
γ	5.12271
β	2.17237 $Å^{-1}$

small difference indicates the successful connection of the narrow observed spectral interval of $a^3\Sigma^+$ to the common asymptote of $a^3\Sigma^+$ and $X^1\Sigma^+$.

5 Discussion and conclusions

From the very large body of highly resolved fluorescence data we could derive a potential curve of $X^1\Sigma^+$ with the correct asymptotic behavior. The extrapolation of the potential for large internuclear separations starts at the largest classical turning 15.281 Å from the high lying level $v'' = 83$, $J'' = 12$ and covers the small extrapolation energy 1.4 cm^{-1} for the rotationless asymptote. If we assume in agreement with the typical estimates of theoreticians that the theoretical values of the dispersion coefficients have an accuracy of about 1% for C_6 (e.g. Ref. [16]) and 10% for the others, then the extrapolation yields the very precise value for the dissociation energy of $D_e = 4954.18 \pm 0.10$ cm^{-1}. The exchange energy does not influence this estimation because at these large internuclear separations its value is already significantly smaller than the dispersion contributions. The new value is in excellent agreement with the first estimation made in [9] but a factor 1000 more precise. Also the newly determined potential function and the Dunham parameters presented in the supplementary *Online material* supersede the earlier published results significantly.

Reporting the dissociation energy with respect to the unobservable minimum of a potential curve introduces a model dependence by the different kinds of setting up the potential curve which results in slight variations of the potential minimum but perfect representation of the vibrational ladder. To remove this ambiguity it is much better to relate the dissociation asymptote to an observable level. Here we use $v'' = 0$, $J'' = 0$, giving the dissociation energy with the symbol D_0 in the generally accepted nomenclature of molecular spectroscopy: $D_0 = 4904.836 \pm 0.10$ cm^{-1}.

With our precise data on the ground state of NaCs and the clear identification of state $a^3\Sigma^+$ by the analyzed hyperfine structure we can check the identification of the observation by Kopystynska et al. [10] to be a vibrational progression of $a^3\Sigma^+$. Because we were also using the laser line 514.5 nm for excitation we simply could compare their recording with ours and our assignment. It became immediately clear that their observation is a part of a progression to the ground state $X^1\Sigma^+$ with high vibrational levels 54 to 58. This explains the small vibrational spacing of 46 cm^{-1} compared to 99 cm^{-1} at the bottom of the potential but much too large to be the vibrational spacing of $a^3\Sigma^+$. And the grouping of this progression, appearing as it would be a separated band, is related to the intensity distribution according to the Franck-Condon factors between $E^1\Sigma^+$ and $X^1\Sigma^+$ observed in this experiment.

The reported potential functions for both electronic states at the atomic ground state asymptote Na($3s$) and Cs($6s$) and the observation that the combined atomic hyperfine structure of Na and Cs describes the molecular hyperfine structure also for low vibrational levels allow model calculation of cold collisions between mixed alkali systems. Scattering lengths are about 1200 au and 65 au for the singlet and triplet state, respectively (1 au = 0.529 Å). The s-wave collisions at the lowest hyperfine asymptote $f(\mathrm{Na}) = 1 + f(\mathrm{Cs}) = 3$ will be described by the scattering lengths of 49 au, 52 au and 57 au for total angular momenta of $f = 2$, 3, and 4, respectively. These values are reported here for giving the reader the opportunity to scale his estimates or analysis of experiments. But certainly refinements of these values must be searched for before a quantitative description of the mixed species interaction will be achieved.

The recent success in photoassociation of ultra cold heteronuclear alkalis, like RbCs [7], clearly asks for detailed knowledge about the excited electronic states, especially for the polar systems. The theoretical results as given in Figure 1 show interesting avoided crossings in the potential curves, which originate from the ion pair configuration. Because the avoided crossings are very strong, the ion pair contribution is widely spread in the configurations, which is probably characteristic for heteronuclear species compared to the homonuclear ones [20]. Thus, one can expect that photoassociation can also be observed via the long range branches in the states $C^1\Sigma^+$ and $E^1\Sigma^+$ which might allow a direct path to the production of ultra cold polar molecules in the ground state with low vibrational levels.

During the present experiment we were collecting a large set of excited levels the assignment of which is started (compare the compilation in the supplementary *Online material*), but needs a fairly deep theoretical analysis because of perturbations and not yet clear vibrational structure. Because we were able to observe through the excitation of the state $E^1\Sigma^+$ very long vibrational progressions which lead to outer turning points up to 15.3 Å the description of the intensity ratio will then give a clear picture of the variation of electronic transition moment for E–X transitions, and thus the character of the configuration changes in the E state.

The work is supported by DFG through SFB 407 and European Graduate College 665 and by EC through the Network "Cold Molecules". O.D., M.T., and R.F. acknowledge the support by the NATO SfP 978029 Optical Field Mapping grant and by the EC 5th Frame Growth Grant G1MA-CT-2002-04063. A.P. acknowledges the support from the Alexander von Humboldt Foundation.

References

1. J.P. Shaffer, W. Chalupczyk, N.P. Bigelow, Phys. Rev. A **60**, R3365 (1999)
2. G. Ferrari, M. Inguscio, W. Jastrzebski, G. Modugno, G. Roati, A. Simoni, Phys. Rev. Lett. **89**, 53202 (2002)
3. Z. Hadzibabic, C.A. Stan, K. Dieckmann, S. Gupta, M.W. Zwierlein, A. Görlitz, W. Ketterle, Phys. Rev. Lett. **88**, 160401 (2002)
4. S.B. Weiss, M. Bhattacharya, N.P. Bigelow, Phys. Rev. A **68**, 042708 (2003)
5. M.A. Baranov, M.S. Mar'enko, Val.S. Rychkov, G.V. Shlyapnikov, Phys. Rev. A **66**, 013606 (2002)
6. K. Goral, L. Santos, M. Lewenstein, Phys. Rev. Lett. **88**, 170406 (2002)
7. A.J. Kerman, J.M. Sage, S. Sainis, T. Bergeman, D. DeMille, Phys. Rev. Lett. **92**, 033004 (2004)
8. M. Korek, A.R. Allouche, K. Fakhreddine, A. Chaalan, Can. J. Phys. **78**, 977 (2000)
9. U. Diemer, H. Weickenmeier, M. Wahl, W. Demtröder, Chem. Phys. Lett. **104**, 489 (1984)
10. A. Kopystynska, C. Gabbanini, S. Gozzini, M. Biagini, L. Moi, Phys. Lett. A **159**, 266 (1991)
11. O. Allard, A. Pashov, H. Knöckel, E. Tiemann, Phys. Rev. A **66**, 42503 (2002)
12. O.Docenko, M. Tamanis, R. Ferber, A. Pashov, H. Knöckel, E. Tiemann, Phys. Rev. A **69**, 042503 (2004)
13. F. Engelke, H. Hage, U. Sprick, Chem. Phys. **88**, 443 (1984)
14. C. Samuelis, E. Tiesinga, T. Laue, M. Elbs, H. Knöckel, E. Tiemann, Phys. Rev. A **63**, 012710 (2000)
15. S.G. Porsev, A. Derevianko, J. Chem. Phys. **119**, 844 (2003)
16. A. Derevianko, J.F. Babb, A. Dalgarno, Phys. Rev. A **63**, 052704 (2001)
17. H. Knöckel, B. Bodermann, E. Tiemann, Eur. Phys. J. D **28**, 199 (2004)
18. X. Wang, J. Magnes, A.M. Lyyra, A.J. Ross, F. Martin, P.M. Dove, R.J. Le Roy, J. Chem. Phys. **117**, 9339 (2003)
19. E. Arimondo, M. Inguscio, P. Violini, Rev. Mod. Phys. **49**, 31 (1977)
20. T. Laue, P. Pellegrini, O. Dulieu, C. Samuelis, H. Knöckel, F. Masnou-Seeuws, E. Tiemann, Eur. Phys. J. D **26**, 173 (2003)